



Contents lists available at ScienceDirect

## Spectrochimica Acta Part A: Molecular and Biomolecular Spectroscopy

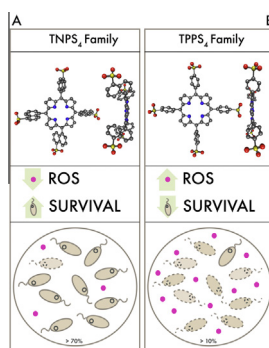
journal homepage: [www.elsevier.com/locate/saa](http://www.elsevier.com/locate/saa)Influence of charge and metal coordination of *meso*-substituted porphyrins on bacterial photoinactivationTamara Zoltan<sup>a,\*</sup>, Franklin Vargas<sup>a</sup>, Verónica López<sup>a</sup>, Valery Chávez<sup>b</sup>, Carlos Rivas<sup>a</sup>, Álvaro H. Ramírez<sup>c</sup><sup>a</sup> Laboratorio de Fotoquímica, Centro de Química, Instituto Venezolano de Investigaciones Científicas I.V.I.C., Apartado 20632, Caracas 1020-A, Venezuela<sup>b</sup> Laboratorio de Bioquímica Celular, Centro de Microbiología y Biología Celular, Instituto Venezolano de Investigaciones Científicas I.V.I.C., Apartado 20632, Caracas 1020-A, Venezuela<sup>c</sup> Laboratorio de Biología de virus, Centro de Microbiología y Biología Celular, Instituto Venezolano de Investigaciones Científicas I.V.I.C., Apartado 20632, Caracas 1020-A, Venezuela

## HIGHLIGHTS

- Were synthesized and characterized 8 *meso* substituted porphyrins with different substituents.
- Effect of charges and metal coordination in their photochemical characteristics was studied.
- We performed a detailed study of photoinduced antibacterial structure–activity.
- It was obtained a relation among the structural integrity, ROS production and antibacterial activity.

## GRAPHICAL ABSTRACT

**A:** The series of TNPS<sub>4</sub> have higher structural deformity, low production of ROS and reduced antibacterial activity. **B:** The series of TPPS<sub>4</sub> have a low structural deformity, high production of ROS and the greater antibacterial activity.



## ARTICLE INFO

## Article history:

Received 23 May 2014

Received in revised form 7 July 2014

Accepted 17 July 2014

Available online 1 August 2014

## Keywords:

Photoinactivation

Water-soluble metallic porphyrins

Reactive oxygen species

*Escherichia coli*

Metal and charge effect

## ABSTRACT

The photodynamic effect of *meso*-substituted porphyrins with different charges and metal ions: *meso*-tetraphenylporphyrin tetrasulfonate **1**, its nickel **2** and zinc complexes **3**; *meso*-tetranaphthylporphyrin tetrasulfonate **4**, and its zinc complex Zn **5**; and tetra pyridyl ethylacetate porphyrins **6** and their nickel **7** and zinc **8** complexes, were synthesized and studied their antimicrobial activity against *Escherichia coli*. Fluorescence quantum yields ( $\Phi_F$ ) were measured in water using reference TPPS<sub>4</sub>, obtaining higher values for complexes **3** and **4**. The singlet oxygen  $\Phi_A$  were measured using histidine as trapping singlet oxygen and Rose Bengal as a reference standard. Complexes **1**, **2** and **6** have the highest quantum yields of singlet oxygen formation, showing no relation with the peripheral charges and efficiency as Type II photosensitizers. Meanwhile complexes **3**, **8** and **4** were the most efficient in producing radical species, determined with their reaction with NADH. The photoinduced antibacterial activity of complex was investigated at different concentrations of the photosensitizers with an irradiation time of 30 min. The higher antibacterial activities were obtained for the complexes **1–3** that are those with greater production of ROS and minor structural deformations. Complexes **7** and **8** had moderate activity, while **4–6** a low activity. Thus, in this work demonstrates that the production of ROS and structural deformations due to peripheral substituents and metal coordination, influence the activity of the complexes studied. Therefore, is important to perform comprehensive study physics and structurally when predicting or explain such activity.

© 2014 Elsevier B.V. All rights reserved.

\* Corresponding author.

E-mail address: [tzoltan@ivic.gob.ve](mailto:tzoltan@ivic.gob.ve) (T. Zoltan).

## Introduction

Due to the wide variety of pathogens and how fast their evolutionary changes to become resistant, the field of antimicrobial chemotherapy is an area of study in constant development. Photodynamic therapy (PDT) has been successfully applied in treating cancer as well as in non-cancerous condition [1,2]. Furthermore, there has also been an increasing interest in the application of PDT in the treatment of infectious diseases [3–5]. PDT involves the use of non-toxic dyes, which act as photoactive drugs called photosensitizers (PS) with the visible light of the proper wavelength to excite the PS. The light raises the PS to an excited state, which then interacts with oxygen, leading to the formation of reactive oxygen species (ROS) such as singlet oxygen, resulting in cytotoxicity and direct cell kill [6].

New developments in PDT applications are several approaches, which innovate in the design of PS is very wide. The chemical structure of a photosensitizer, charge and hydrophobicity influences their efficiency of ROS productions and determines how it interacts with itself and with its environment. Theoretically, photosensitizers can be properly designed a function of its chemical structure, but more realistically their effectiveness is determined as a function of the targets to be confronted [7].

The design of porphyrins as PS with microbial activity PDT has been extensively studied mainly focused on develop cationic complexes, due to possibility of interaction with the cell membrane [8,9]. The development of neutral or anionic porphyrins, regardless of their efficiency to produce reactive oxygen species, does not receive great attention because of its low interaction on the membrane [10,11]. Many of those studies report that the latter porphyrins have negligible activity against Gram-negative bacteria such as *Escherichia coli* [12]. It is important to note that the experimental method, bacterial washes are performed system before irradiation, thereby eliminating the PS not attached to the bacteria [13,14]. Taking into account that in large-scale applications, such as in wastewater treatment, these washings not performed, the efficiency of ROS production in the entire system plays an important role in bacterial photoinactivation. Thus, evaluating new photosensitizers on bacterial cultures without pre-irradiation washes, would allow obtaining information about the system under real operating conditions. In this sense, in this work the synthesis and photochemical characterization 8 hydrophilic porphyrins were performed. The aim of this paper is to examine their efficiency as PS in cultures of *E. coli* (no previous washes), and the impact of structural changes in this efficiency.

In this paper the synthesis of the following water-soluble porphyrins is presented: *meso*-tetraphenylporphyrin (TPP) tetrasulfonate ( $S_4$ ): (TPPS<sub>4</sub>, **1**), its nickel (TPPNiS<sub>4</sub>, **2**) and zinc complexes (TPPZnS<sub>4</sub>, **3**) as well as the *meso*-tetranaphthylporphyrin tetrasulfonate (TNPS<sub>4</sub>, **4**) its Zn complexes (TNPZnS<sub>4</sub>, **5**) and tetra pyridyl ethylacetate porphyrins (TPyEtAcP, **6**) and their Ni and Zn complexes (TPyEtAcPNi, **7**; TPyEtAcPZn, **8**). Studied photophysical properties of absorption, fluorescence emission and the photochemical characteristic of singlet oxygen generation and oxygen free radicals by synthesized porphyrins are compared in dependence on the chemical structure. Finally, a comparison of the photochemical properties of the synthesized compounds and its efficiency in the photoinduced antibacterial activity is performed.

## Materials and methods

### Chemicals

All analytical or HPLC grade solvents were obtained from Merck (Darmstadt, Germany) and used without further purification.

Benzaldehyde,  $\alpha$ -naftaldehyde, chloro ethyl acetate, pyrrole, propionic acid, tetra-pyridyl porphyrin, chloroform, histidine, Rose Bengal, horseradish peroxidase (HRP), nicotinamide adenine dinucleotide phosphate reduced form (NADPH), and *p*-nitrosodimethyl aniline were purchased from Sigma–Aldrich (St. Louis, MO, USA). 3-Aminophthalhydrazide (Luminol) and hydrogen peroxide, 30 wt.% solution in water, were purchased from Aldrich (Milwaukee, USA). Phosphate buffered saline solution (PBS) pH 7.4 (0.01 mol l<sup>-1</sup> phosphate buffer and 0.135 mol l<sup>-1</sup> NaCl) was prepared daily before each experiment.

<sup>1</sup>H NMR and <sup>13</sup>C NMR spectra were recorded with a Bruker Avance 500 and 300 MHz respectively, in chloroform-*d* with tetramethylsilane (Me<sub>4</sub>Si) as an internal standard. Chemical shifts ( $\delta$ ) are given in parts per million. Infrared spectroscopy (IR) spectra were performed using a Nicolet Magna 560 FT-IR spectrometer. ElectroSpray Ionization mass spectra and MS/MS spectra were obtained with a Thermo-Finnigan TSQ Quantum Ultra AM spectrometer coupled to a HPLC ElectroSpray (ESI). Elemental analyses were performed in a Fisons Instrument EA-1108. The samples were prepared by addition of the compound of interest to water. The absorption spectra were recorded on a Perkin Elmer Lambda-35 UV-Vis spectrophotometer. The fluorescence spectra and the quantum yields were registered in a Perkin Elmer LS-45.

### Synthesis of the porphyrins derivatives

#### Tetraphenyl porphyrins (TPP)

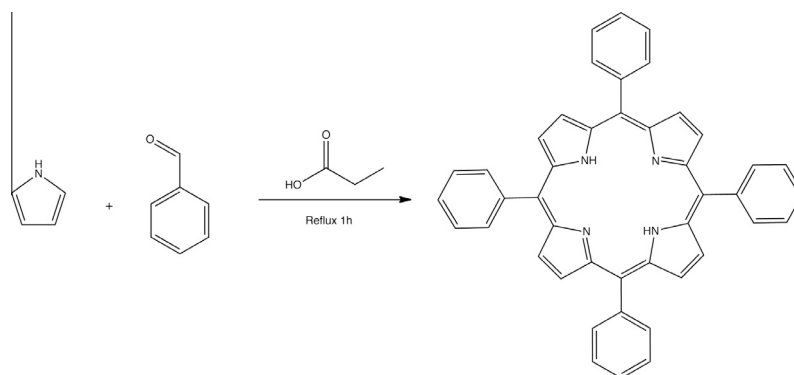
The synthesis of TPP (Scheme 1) was carried out following the experimental procedure reported by Alder and coworkers [15] with some modifications: benzaldehyde (0.67 mol) and pyrrole (0.65 mol) were added simultaneously to refluxing propionic acid (200 ml) and the mixture was refluxed for 1 h before being allowed to cool and stand at room temperature overnight. The product was filtered off and washed with water and methanol to give purple crystals. Yield 20% (20.5 g). **F.T-IR** (KBr, thin film)  $\nu_{\max}$  (cm<sup>-1</sup>): 3309 (N–H); 3047 (C=C); 2361 (C=N); 1593, 1466 (aromatic C=C); 698 (C–H). **UV-vis** (1.0 × 10<sup>-5</sup> mol l<sup>-1</sup> in CHCl<sub>3</sub>),  $\lambda_{\max}$  (nm): 419, 515, 550, 590, 674; **<sup>1</sup>H NMR** (500 MHz, CDCl<sub>3</sub>)  $\delta$  = ppm: 8.87 (s, 8H, H-pyrrolic), 8.21–8.28 (d, *J* = 5.0 Hz, 8H, *o*-phenyl), 7.72–7.85 (m, 12H, H-phenyl), –2.73 (s, NH). **<sup>13</sup>C NMR** (125 MHz, CHCl<sub>3</sub>)  $\delta$  = ppm: 142.21 (2C-phenyl), 134.6 (CH-*o*-phenyl), 131.15 (CH-pyrrolic), 127.74 (2C-pyrrolic), 126.72 (2CH-phenyl), 120.18 (2C).

#### Tetranaphthylporphyrins (TNP)

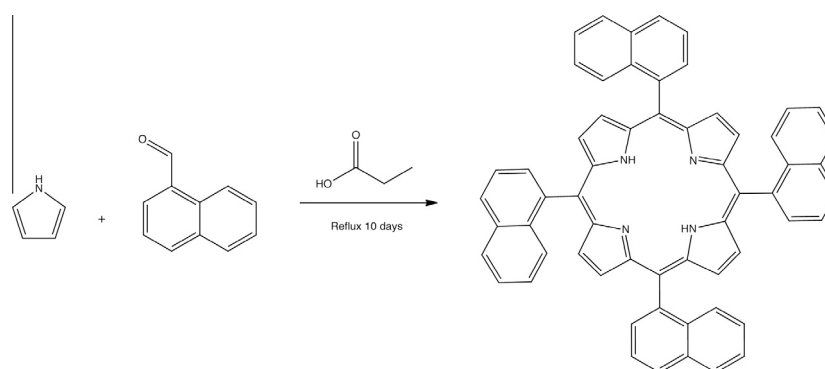
The synthesis of TNP (Scheme 2) was carried out following the experimental procedure reported by Regimol and coworkers [16] with some modifications: benzaldehyde (0.10 mol) and pyrrole (0.14 mol) were added simultaneously to refluxing propionic acid (100 ml). The reaction mixture was left at reflux for a ten days, after which it was allowed to cool to room temperature, and then it was kept at 5 °C overnight. The product was filtered off and washed with water and methanol and the solid obtained was purified by preparative chromatography on silica plates, using chloroform as mobile phase, yielding purple crystals. Yield of 19.8% (5.44 g). **F.T-IR** (KBr, thin film)  $\nu_{\max}$  (cm<sup>-1</sup>): 3432 (N–H), 2357 (C=N), 3048 (C=C), 1568, 1499 (aromatic C=C), 1021 (C–H). **UV-vis** (1.0 × 10<sup>-5</sup> mol l<sup>-1</sup> in CHCl<sub>3</sub>),  $\lambda_{\max}$  (nm): 423. **<sup>1</sup>H NMR** (500 MHz, CDCl<sub>3</sub>)  $\delta$  = ppm: 8.47 (d, 8H, *J* = 4.5 Hz, H-pyrrolic), 8.28–7.73 (m, 28H, H-naphthalene), –2.76 (s, 2H, NH). MS (APCI) *m/z*: 815.22 (M + H)<sup>+</sup>, (cal: M: C<sub>60</sub>H<sub>38</sub>N<sub>4</sub> = 814.97).

#### Tetrapiridyl ethylacetate porphyrins

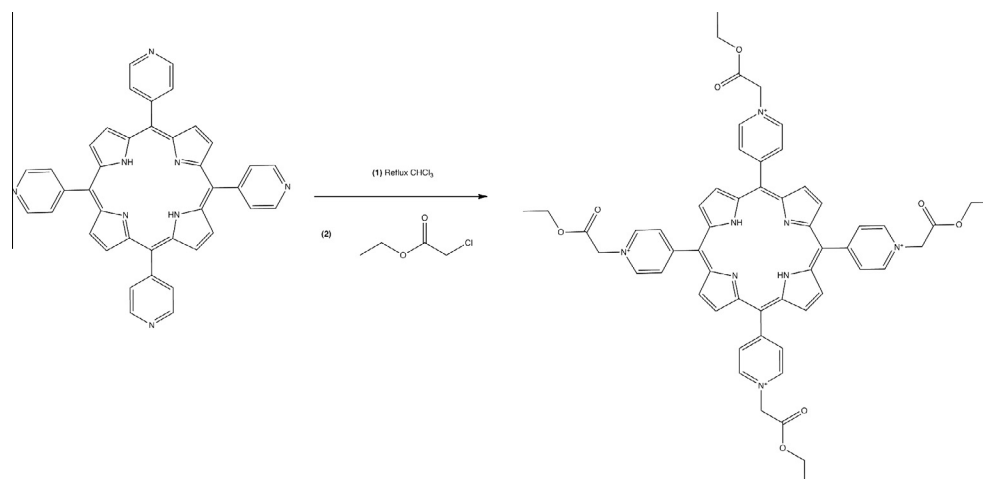
(TPyEtAcP, **6**): The synthesis of water-soluble porphyrin TPyEtAcP (Scheme 3) was performed according to changes in the methodology reported by Berezin and coworkers [17]: tetrapiridyl



**Scheme 1.** Synthesis of tetraphenyl porphyrins (TPP).



**Scheme 2.** Synthesis of tetranaphthylporphyrins (TNP).



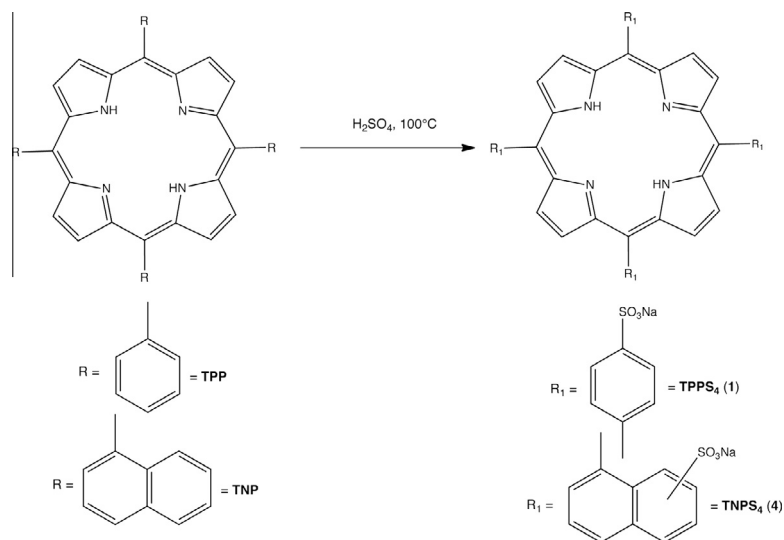
**Scheme 3.** Synthesis of tetrapiridyl ethylacetate porphyrins (TPyEtAcP).

porphyrin (0.16 mmol) in 30 mL of  $\text{CHCl}_3$  was placed under reflux. After the reflux was stable an excess of ethyl chloroacetate (6 mL) was added drop wise. The mixture was left at reflux for 48 h; after that which it was evaporated to dryness, and the product obtained was washed with  $\text{CHCl}_3$  to remove starting materials, thus getting dark pink crystals. Yield of 69.6% (0.125 g). **F.T-I.R** (KBr, thin film)  $\nu_{\text{max}}$  ( $\text{cm}^{-1}$ ): 3318, 3090, 1632, 1561, 1502, 1459, 1365, 1285, 1093, 1000, 716, 657. **UV-vis** ( $1.0 \times 10^{-5}$  mol  $\text{l}^{-1}$  in  $\text{H}_2\text{O}$ , pH 7.2),  $\lambda_{\text{max}}$  (nm): 422, 519, 557, 584, 641.  **$^1\text{H NMR}$**  (500 MHz,  $\text{DMSO-d}_6$ )  $\delta$  = ppm: 9.66–9.63 (d, 8H,  $J$  = 5.0 Hz, H-pyridyl), 9.13–9.10 (d, 8H,  $J$  = 5.0 Hz, H-pyridyl), 8.29 (s, 4H, H-acetate), 6.13 (s, 2H, H-pyrrolic), 4.45–4.41 (c, 8H,  $J$  = 5.50 Hz,  $\text{CH}_2$ -Ethyl), 1.42–1.40 (t, 12,

$J$  = 5.50 Hz,  $\text{CH}_3$ -Ethyl),  $-3.02$  (s, NH).  **$^{13}\text{C NMR}$**  (125 MHz,  $\text{DMSO-d}_6$ )  $\delta$  = ppm: 14.5 ( $\text{CH}_3$ -Ethyl), 60.57 ( $\text{CH}_2$ - $\text{N}^+$ ), 62.99 ( $\text{CH}_2$  Ethyl), 115.81 (2C-pyrrolic), 129.52 (2CH-pyrrolic), 124.6 (2C pyridyl), 145.4 (C- $\text{N}^+$ -Pyridyl), 148.86 (C-*meso*-porphyrin), 158.24 (C-*meso*-pyridyl), 167.06 (C-acetate). **MS = m/z**: 791.23 (M-2EtAc) $^+$  (cal: M - 2EtAc ( $\text{C}_{48}\text{H}_{38}\text{N}_8\text{O}_4 + \text{H}$ ) = 791.31).

#### General procedure of the sulfonation reaction

The synthesis of TPPS<sub>4</sub>, **1** (or TNPS<sub>4</sub>, **4**) was carried out following the general procedure with some modifications, described by Srivastava and coworkers [18] (Scheme 4). *Meso*-tetraphenylporphyrin (1.6 mmol, 1 g) was mixed with 20 ml of concentrated sulfuric



**Scheme 4.** General procedure of the sulfonation reaction.

acid. The mixture was heated at 100 °C, controlling the temperature for 24 h. Afterward, the solution at room temperature, was filtered through a glass filter funnel and the filtrate was diluted carefully to 500 mL with water. The dilute green solution was heated and calcium oxide (CaO) was added slowly with stirring until the solution changed to a permanent purple color. Calcium sulfate was filtered off and washed with a minimum quantity of hot water, which was then combined with the filtrate. Crushed Dry Ice was added to the filtrate and was filtered. The filtrate was concentrated to a small volume (about 100 mL) and the pH of the final warm solution was regulated in 9 with sodium carbonate solution. Calcium carbonate was removed by filtration and washed with water, which was then combined with the filtrate. The resulting solution was carried to dryness and the solid dissolved in MeOH, filtered to remove excess carbonate formed. The resulting solution was evaporated and recrystallized with acetone to get purple crystals highly soluble in water of tetrasodium *meso*-tetra (*p*-sulfophenyl) porphine, TPPS<sub>4</sub> (or tetrasodium *meso*-tetra (*p*-sulfonaphthyl) porphine, TNPS<sub>4</sub>).

TPPS<sub>4</sub> **1**, yield 57.8% (0.946 g). **F.T-IR** (KBr, thin film)  $\nu_{\max}$  (cm<sup>-1</sup>): 3360, 3320, 3010, 1940, 1630, 1548, 1390, 1300, 1110, 1060, 995, 739, 700, 638 cm<sup>-1</sup>. **UV-vis** ( $1.0 \times 10^{-5}$  mol l<sup>-1</sup> in H<sub>2</sub>O, pH 7.2),  $\lambda_{\max}$  (nm): 413, 515, 633, 579 553. **<sup>1</sup>H NMR** (500 MHz, DMSO-d<sub>6</sub>)  $\delta$  = ppm: 8.81 (s, 6H, H-pyrrolyc), 8.11–8.21 (d, 8H, *J* = 10 Hz H-*m*-phenyl), 7.8–8.05 (d, 8H, *J* = 10 Hz H-*o*-phenyl), –2.97 (s, NH). **<sup>13</sup>C NMR** (125 MHz, DMSO-d<sub>6</sub>)  $\delta$  = ppm: 148.1 (2C-phenyl), 141.7 (CH-*o*-phenyl), 134.1 (C=N-pyrrolic), 131.7 (2C-pyrrolic), 124.6 (CH-*m*-phenyl), 120.1 (2C). TNPS<sub>4</sub> **4**, yield 85.73% (0.578 g). **UV-vis** ( $1.0 \times 10^{-5}$  mol l<sup>-1</sup> in H<sub>2</sub>O, pH 7.2),  $\lambda_{\max}$  (nm): 419, 633, 578, 556.

#### General procedure of the metallation reaction

The reaction was carried out as described by Herrman and coworkers [19] with modifications (Scheme 5): 50 mg of TPPS<sub>4</sub>, TNPS<sub>4</sub> or TPyEtAc, was added to 100 ml of refluxing distilled and deionized water, containing 1 g of metal oxide (ZnO or NiO). The mixture was refluxed for 24 h monitoring the progress of the reaction until the fusion the four bands Q in two. After that, the mixture was filtrated on a 0.22 μ Millipore filter and evaporated to dryness under reduced pressure dried at 120 °C under vacuum, obtained the metalloporphyrins. Nickel *meso*-tetrasulfonatophenyl porphyrin (TPPNiS<sub>4</sub> **2**), yield 42.3% (0.482 g). **UV-vis** ( $1.0 \times 10^{-5}$  mol l<sup>-1</sup> in H<sub>2</sub>O, pH 7.2), ( $\lambda_{\max}$  nm). 414, 515, 553. Zinc *meso*-tetra-

sulfonatophenyl porphyrin (TPPZnS<sub>4</sub> **3**), yield 71.4% (0.764 g). **UV-vis** ( $1.0 \times 10^{-5}$  mol l<sup>-1</sup> in H<sub>2</sub>O, pH 7.2), ( $\lambda_{\max}$  nm). 421, 556, 595. Zinc *meso*-tetrasulfonatophenyl porphyrin (TNPZnS<sub>4</sub> **5**) with a yield 85.73% (0.578 g). **UV-vis** ( $1.0 \times 10^{-5}$  mol l<sup>-1</sup> in H<sub>2</sub>O, pH 7.2),  $\lambda_{\max}$  (nm): 426, 467, 557, 594. Nickel *meso*-tetrapiridyl ethyl acetate porphyrin (TPyEtAcPnNi **7**), yield 54.6% (0.288 g). **UV-vis** ( $1.0 \times 10^{-5}$  mol l<sup>-1</sup> in H<sub>2</sub>O, pH 7.2),  $\lambda_{\max}$  (nm): 418, 532, 563. **MS = m/z**: 674.09 (M-4EtAc + 2H)<sup>-</sup>, (calc M-4EtAc + 2H: (C<sub>40</sub>H<sub>24</sub>N<sub>8</sub>Ni) = 674.15). Zinc *meso*-tetrapiridyl ethylacetate porphyrin (TPyEtAcPzZn **8**) yields 54.6% (0.288 g). **UV-vis** ( $1.0 \times 10^{-5}$  mol l<sup>-1</sup> in H<sub>2</sub>O, pH 7.2),  $\lambda_{\max}$  (nm): 437, 564 608. **MS = m/z**: 681.05 (M + H)<sup>+</sup>, (calc: M + H: (C<sub>40</sub>H<sub>24</sub>N<sub>8</sub>Zn) = 681.15). The NMR (<sup>1</sup>H and <sup>13</sup>C) and I.R. spectra showed no significant differences with those obtained in the compounds without metal.

#### Irradiation

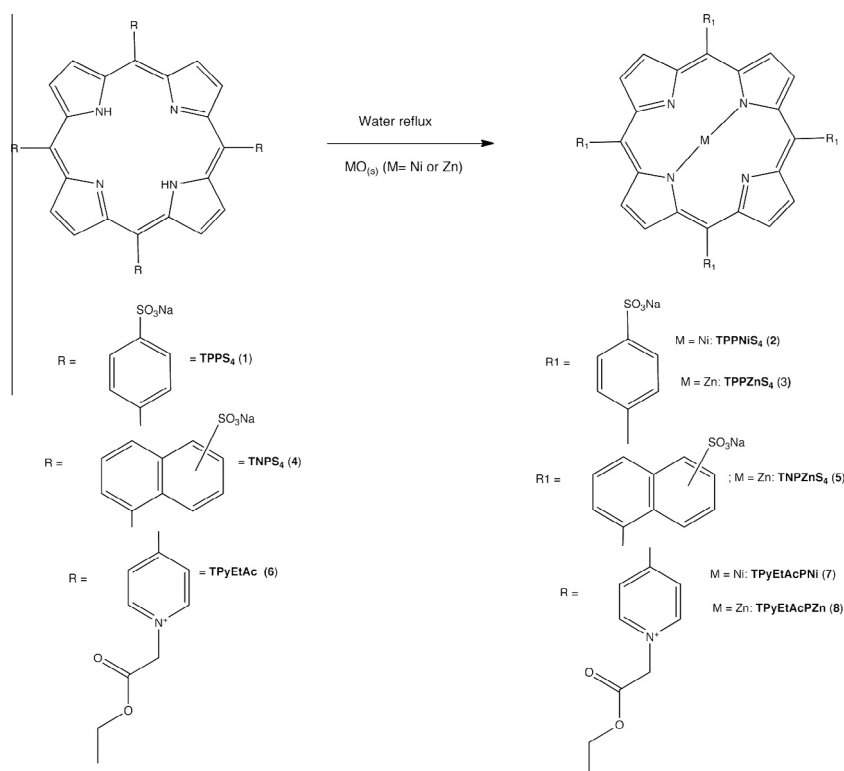
All processes of irradiation were carried out using an illuminator LuzChem LZC 4V Photoreactor equipped with 14 lamps with emission in the UV-A (320–400 nm, 3.3 mW cm<sup>-2</sup>) and in the visible, keeping a distance of 10 cm between the lamp surface and the solution flask, varying the time periods of exposure at 37 °C under continuous shaking. The radiation dose was 4.5 J/cm<sup>2</sup> as measured with a model of UVX Digital Radiometer after 1 h of continued illumination.

#### Fluorescence quantum yields

The relative quantum yields of fluorescence for porphyrins complexes (**1–8**) were determined at room temperature by the comparative method using Rose Bengal as standard (at a concentration of  $1 \times 10^{-6}$  mol l<sup>-1</sup> in ethanol; fluorescence quantum yield, 0.11) or else with that of quinine bisulfate in 0.05 mol l<sup>-1</sup> H<sub>2</sub>SO<sub>4</sub> (fluorescence quantum yield, 0.55) [20]. Fluorescence quantum yields ( $\Phi_F$ ) were determined using the Eq. (1) [21]:

$$\Phi_F = \Phi_F(\text{Std}) \frac{F_{\text{Std}} A_{\text{Std}} \eta^2}{F_{\text{Std}} A \eta_{\text{Std}}^2} \quad (1)$$

where *F* and *F*<sub>Std</sub> are, respectively, the areas under the fluorescence curves of the samples (**1–8**) and the standard. *A* and *A*<sub>Std</sub> are the respective absorbance of the sample and of the standard at the excitation wavelengths.  $\eta$  and  $\eta_{\text{Std}}$  are the refractive indices of solvents used, for the sample and the standard respectively.



**Scheme 5.** General procedure of the metallation reaction.

### Singlet oxygen generation

Singlet oxygen was measured by photosensitized degradation of L-histidine with synthetic porphyrins (**1–8**,  $4 \times 10^{-5}$  mol l<sup>-1</sup>) [22,23]. In a typical experiment, a mixture (equal volumes and concentrations) of porphyrins complex (**1–8**) and L-histidine (in

phosphate buffer 0.01 M, pH 7.4) was irradiated with visible light (>420 nm) under oxygen and gentle magnetic stirring for different periods of time up to 30 min (5, 10, 15, 20, 25 and 30) with the respective controls been protected from light. The concentration of L-histidine was determined by a colorimetric reaction using phosphate buffer, sulfanilic acid, sodium nitrite, sodium carbonate and ethanol as reagents. The optical density was read on a spectrophotometer at 440 nm against a blank reagent (a modified Pauly reaction), and by bleaching of *p*-nitrosodimethylaniline [19,24].

Another “trap” method has been successfully used to detect the generated <sup>1</sup>O<sub>2</sub> in a variety of samples. This method is based on following the consumption of a chemical trap (Furfuryl alcohol, FFA) that reacts with singlet oxygen. The consumption of FFA was followed by HPLC using a 90:10 H<sub>2</sub>O/CH<sub>3</sub>CN mobile phase composition. The wavelength detection used for monitoring FFA consumption was at 222 nm. Rose Bengal a well known <sup>1</sup>O<sub>2</sub> sensitizer, was used as a standard for comparison with synthetic porphyrins for <sup>1</sup>O<sub>2</sub> formation, under same conditions of photolysis [24,25].

### Quantum yields of singlet oxygen

Quantum yields of singlet oxygen photogeneration were determined in air (no oxygen bubbled) using the relative method with Rose Bengal as reference and histidine as a chemical quencher of singlet oxygen, from Eq. (2):

$$\Phi_{\Delta} = \Phi_{\Delta}^{Std} \frac{W}{W^{Std}} \quad (2)$$

where  $\Phi_{\Delta}^{Std}$  are the singlet oxygen quantum yields for the standard, Rose Bengal in water (0.79) [26].  $W$  and  $W^{Std}$  are the *p*-nitrosodimethylaniline photobleaching rates in the presence of the porphyrins complexes and the standard, respectively [27].

**Table 1**  
Absorption spectra of Porphyrins **1–8**, in water ( $1 \times 10^{-5}$  mol l<sup>-1</sup>).

Porphyrins	Soret band (nm) ( $\epsilon \times 10^3$ (mol l <sup>-1</sup> ) <sup>-1</sup> cm <sup>-1</sup> )	Q bands (nm)
TPPS <sub>4</sub> ( <b>1</b> )	413.32 (129)	515.53 552.40 579.58 633.24
TPPS <sub>4</sub> Ni ( <b>2</b> )	413.91 (51)	515.53 552.87
TPPS <sub>4</sub> Zn ( <b>3</b> )	421.38 (174)	556.51 595.34
TNPS <sub>4</sub> ( <b>4</b> )	419.22 (107)	516.65 556.05 578.06 632.82
TNPS <sub>4</sub> Zn ( <b>5</b> )	426.23 (126)	556.96 594.79
TPPyEtAcP ( <b>6</b> )	422.94 (125)	519.18 557.97 584.73 641.03
TPPyEtAcPNI ( <b>7</b> )	418.08 (77)	532.50 562.80
TPPyEtAcPZn ( <b>8</b> )	436.96 (153)	563.97 608.47

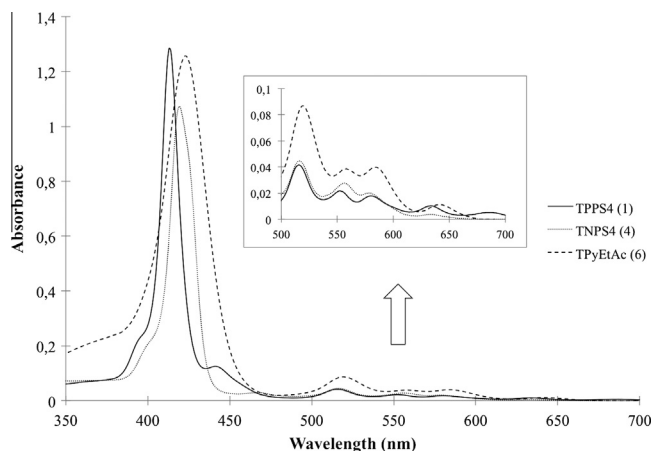


**Fig. 1.** Absorption spectra of: *meso*-tetraphenylporphyrin tetrasulfonate (—TPPS<sub>4</sub>, **1**), *meso*-tetranaphthylporphyrin tetrasulfonate (---TNPS<sub>4</sub>, **4**), *meso*-tetrapiridyl ethylacetate porphyrin (· · ·TPyEtAcP, **6**).

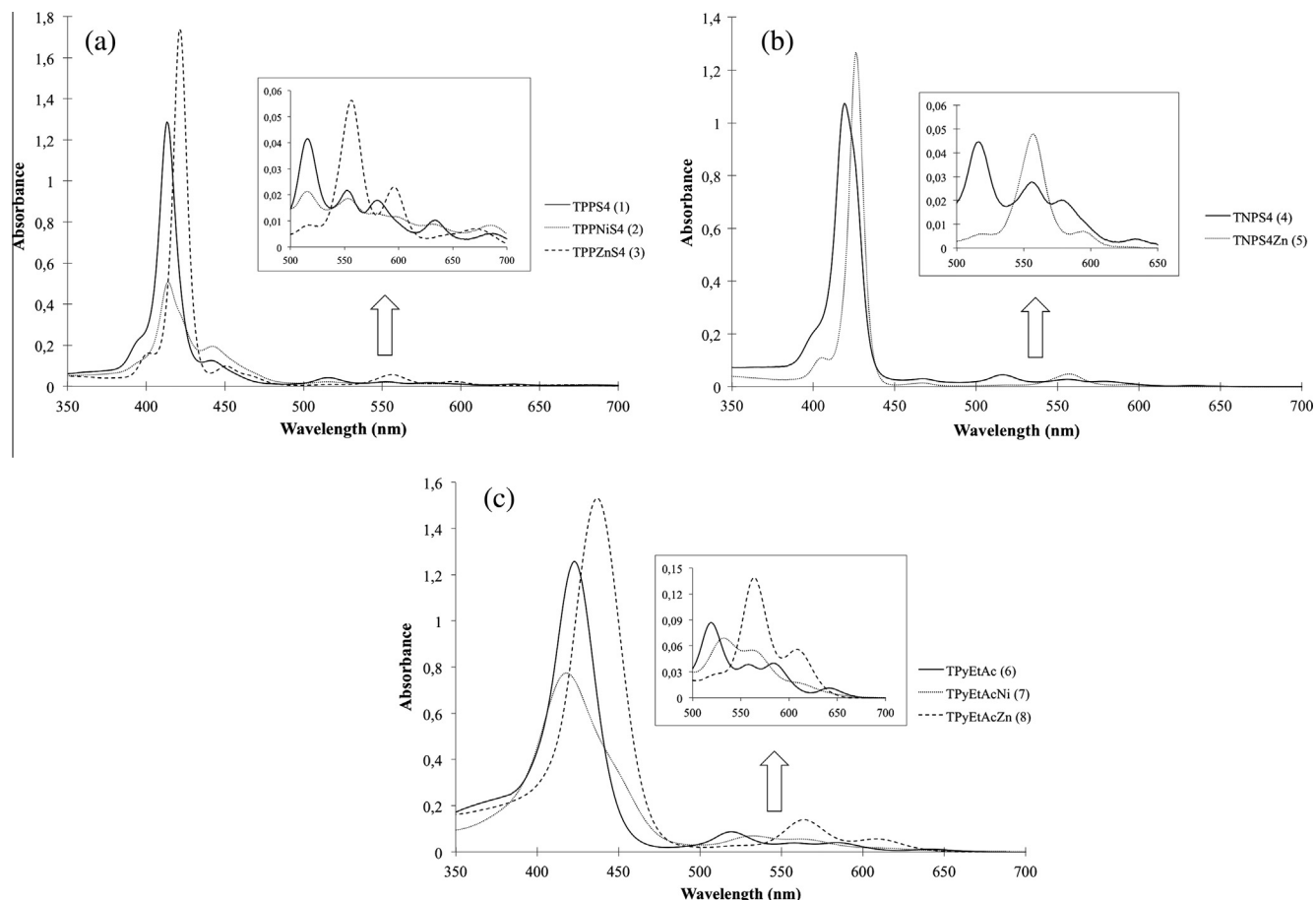
#### Detection of others reactive oxygen species

Chemiluminescence (CL) was generated in cell-free systems; H<sub>2</sub>O<sub>2</sub>-induced CL (as a blank): H<sub>2</sub>O<sub>2</sub> (3.5 mmol l<sup>-1</sup>) was added to phosphate buffered saline solution (PBS, 0.01 mol l<sup>-1</sup> phosphate buffer and 0.135 mol l<sup>-1</sup> NaCl, pH 7.2) and luminol (250 μmol l<sup>-1</sup>,

prepared daily in 2 mol l<sup>-1</sup> of NaOH and diluted with PBS). The porphyrins-induced CL at different concentrations was dispensed after irradiation in presence of NADPH. The generated CL at 37 °C was measured continuously for 10 min in a Luminoskan Ascent luminometer (ThermoLabsystems, Finland) in a 96-well Thermo Labsystems Microtiter plate [28–30].

#### Antibacterial photoactivity

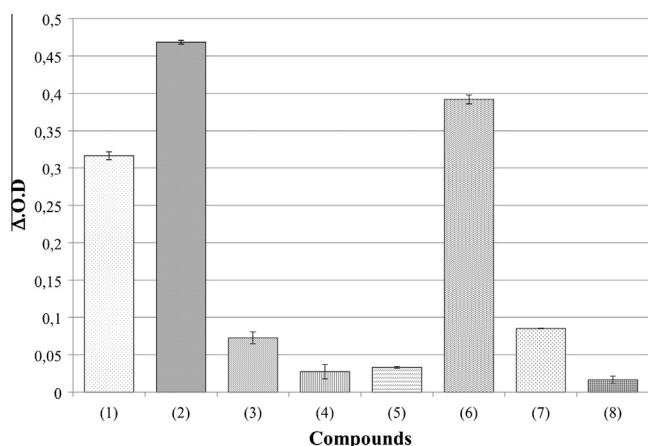
Antibacterial assay was carried out using *E. coli* (ATCC<sup>®</sup> 8739TM [31]) and their proliferation and viability were obtained by chemiluminescence using BacTiter-Glo Microbial Cell (Promega, USA). The compounds used **1–8** were prepared in H<sub>2</sub>O, in a concentration range of 1.0 × 10<sup>-4</sup> to 5.0 × 10<sup>-6</sup> mol l<sup>-1</sup>. Taking into account that different bacteria have different amounts of ATP per cell, and values reported for the ATP level in cells vary considerably. Factors that affect the ATP content of cells such as growth phase, culture medium, and the presence of metabolic inhibitors, can influence the relationship between cell concentration and luminescence. The antibacterial photoactivity was carried out under irradiation with an illuminator LuzChem LZC 4V Photoreactor using 14 lamps with emission in UV-A (320–400 nm with a fluence rate of 3.3 mW cm<sup>-2</sup>, 45.575 Lux seg<sup>-1</sup> and light dose of 5.94 J cm<sup>-2</sup>), keeping a distance of 10 cm between the lamp surface and the solution flask, varying the time periods of exposure at 37 °C under continuous shaking.



**Fig. 2.** Absorption spectra of: (a) *meso*-tetraphenylporphyrin tetrasulfonate (—TPPS<sub>4</sub>, **1**), Nickel *meso*-tetraphenylporphyrin tetrasulfonate (---TPPNiS<sub>4</sub>, **2**), Zinc *meso*-tetraphenylporphyrin tetrasulfonate (· · ·TPPZnS<sub>4</sub>, **3**); (b) *meso*-tetranaphthylporphyrin tetrasulfonate (—TNPS<sub>4</sub>, **4**), Zinc *meso*-tetranaphthylporphyrin tetrasulfonate (---TNPS<sub>4</sub>Zn, **5**) and (c) *meso*-tetrapiridyl ethylacetate porphyrin (—TPyEtAcP, **6**), Nickel *meso*-tetrapiridyl ethylacetate porphyrin (---TPyEtAcPNi, **7**), Zinc *meso*-tetrapiridyl ethylacetate porphyrin (· · ·TPyEtAcPZn, **8**).

**Table 2**  
Relative fluorescence quantum yields ( $\Phi_F$ ) of synthesized compounds 1–8 in water.

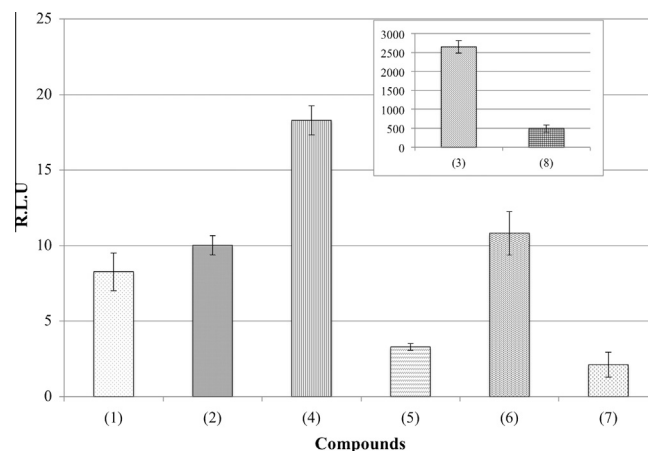
Porphyrins	$\lambda_{exc}$ (nm)	$\lambda_{em}$ (nm)	$\Phi_F$
TPPS <sub>4</sub> (1)	430.58	640.75	0.12 <sup>a</sup>
TPPS <sub>4</sub> Ni (2)	433.96	640.86	0.070
TPPS <sub>4</sub> Zn (3)	436.08	605.11	0.103
TNPS <sub>4</sub> (4)	432.11	639.87	0.07
TNPS <sub>4</sub> Zn (5)	444.96	603.81	0.06
TPyEtAcP (6)	424.66	657.70	0.02
TPyEtAcPNi (7)	450.61	649.23	0.003
TPyEtAcPZn (8)	434.13	631.48	0.044

<sup>a</sup> Reported [41].**Fig. 3.** Effect of 30 min irradiation of the compounds 1 to 8 on the bleaching of *p*-nitrosodimethylaniline in the presence of the histidine at 440 nm.  $\Delta$ O.D. represents the difference in optical density of irradiated samples of compounds 1 to 8.**Table 3**  
Quantum yields ( $\Phi_A$ ) and quantification of singlet oxygen by porphyrins 1–8 using the methodology of the degradation of histidine [22].

Porphyrins	$\Phi_A$	[ <sup>1</sup> O <sub>2</sub> ] (mol/L)	mol <sup>1</sup> O <sub>2</sub> /mol porphyrins
TPPS <sub>4</sub> (1)	0.620	$9.04 \times 10^{-6}$	120.59
TPPS <sub>4</sub> Ni (2)	0.918	$1.34 \times 10^{-5}$	178.48
TPPS <sub>4</sub> Zn (3)	0.142	$2.07 \times 10^{-6}$	27.65
TNPS <sub>4</sub> (4)	0.053	$7.80 \times 10^{-7}$	10.40
TNPS <sub>4</sub> Zn (5)	0.065	$9.48 \times 10^{-7}$	12.65
TPyEtAcP (6)	0.768	$1.12 \times 10^{-5}$	149.31
TPyEtAcPNi (7)	0.167	$2.43 \times 10^{-6}$	32.45
TPyEtAcPZn (8)	0.033	$4.77 \times 10^{-7}$	6.36

**Table 4**  
Production of oxygen free radicals of porphyrins 1–8 as a function of the quantification of H<sub>2</sub>O<sub>2</sub> on the chemiluminescence assay.

Porphyrins	[H <sub>2</sub> O <sub>2</sub> ] (mol l <sup>-1</sup> ± DS) × 10 <sup>-4</sup>	(mol H <sub>2</sub> O <sub>2</sub> /mol porphyrins) ± S.D.
TPPS <sub>4</sub> (1)	1.04 ± 0.08	3 ± 1
TPPS <sub>4</sub> Ni (2)	1.26 ± 0.08	3.8 ± 0.2
TPPS <sub>4</sub> Zn (3)	330 ± 20	999 ± 63
TNPS <sub>4</sub> (4)	2.3 ± 0.1	6.9 ± 0.4
TNPS <sub>4</sub> Zn (5)	0.42 ± 0.03	1.2 ± 0.1
TPyEtAcP (6)	1.4 ± 0.1	4.1 ± 0.5
TPyEtAcPNi (7)	0.27 ± 0.02	0.80 ± 0.05
TPyEtAcPZn (8)	62 ± 1	186 ± 4

**Fig. 4.** Generation of peroxidic species determined by chemiluminescence generates for complexes 1–8. R.L.U. = relative light units. Data are the mean and SEM, ( $n = 4$ ,  $p < 0.05$  vs. control; analysis of variance).

The BacTiter-Glo. Microbial Cell Viability Assay is a homogeneous method to determine the number of viable bacterial cells in culture based in quantification of ATP present; as it well known ATP is an indicator of metabolically active cells. The homogeneous assay procedure involves the addition of a single reagent (BacTiter-Glo Reagent) directly on bacterial cells in LB Broth medium followed by the measurement of luminescence. The luminescent signal is proportional to the amount of ATP present, which in turn is directly proportional to the number of viable cells in culture.

The recorded luminescence signals (Luminescence (R.L.U.: relative light units) represent the mean of three replicates for each measurement. The signal-to-noise ratio was calculated:  $S:N = \text{mean of signal} / \text{mean of background} / \text{standard deviation of the background}$ .

A direct correlation (linear correlation) exists between luminescence measured with the BacTiter-Glo Microbial Cell Viability Assay and the number of cells in culture over five orders of magnitude. Values represent the mean ± S.D. of four replicates for each cell number. The luminescent signal from 50 *E. coli* cells is greater than three standard deviations above the background signal resulting from serum-supplemented medium without cells. There is a linear relationship ( $r^2 = 0.99$ ) between the luminescent signal and the number of cells from 0 to 50,000 cells per well.

#### Statistical treatment of results

At least three independent experiments were performed for each compound except where indicated otherwise. The quantification of results is expressed as a mean ± S.D. standard deviation (S.D.) is obtained from 3 to 4 observations. The level of significance accepted was  $p \leq 0.05$ .

## Results and discussions

### Synthesis and characterization of porphyrins

To synthesize of TPP and TNP were used based methodologies as reported by Alder et al. employing benzaldehyde and 1-naphthaldehyde. Yields obtained for *meso*-substituted porphyrins were approximately 20%, which agrees well with the expected values. The complexes metals free (1, 4 and 6) were obtained with high yields (58–85%). Free complexes were metallized with the respective oxides (ZnO and NiO) in heterogeneous system using water as a solvent. All the porphyrins complexes (1–8) were purified by

column chromatography and pure compounds were obtained, verified by  $^1\text{H}$  NMR and MS spectra.

### Primary photophysical properties of porphyrins 1–8

Fundamental stage of any photochemical process is the absorption of a photon by a photo-excitable molecule. The absorbance and emission spectra of the synthesized complexes provides information for select the wavelength used and the processes of deactivation of their excited states.

The absorption spectra of synthesized porphyrins in water (1–8) show the typical Soret and Q bands of *meso*-substituted porphyrins. The absorption maxima and extinction coefficient of the in water are presented in Table 1.

The absorption spectra of metal-free porphyrins 1, 4 and 6 (Fig. 1) showed a Soret band around 420 nm arising from the transition of  $a_{1u}(\pi) - e_g^*(\pi)$ , and Q bands between 515 and 640 nm corresponding to the  $a_{2u}(\pi) - e_g^*(\pi)$  transition. A small red shift was observed in the Soret band of 4 and 6 with respect to 1, that may be attributed to a slight loss of planarity of the macrocycle due to the peripheral substituents [32]. It has been reported that the magnitude of the red shift is proportional to the extent of the distortion in the planarity of the molecule and depends on both the shape and size of the substituents [33,34]. In this way this loss is attributable to a steric effect of the substituent groups and repulsion effects associated with the positions of the substituents. These effects can be clearly seen in Fig. S1 (supplementary material), where the porphyrin structures were optimized using the Avogadro software [35].

The UV–vis spectra of metal complexes (Fig. 2a–c) shows the characteristic peak of the Soret band and a shift characteristic regarding to the free base analogue of metal complexes with configuration  $d^6-d^{10}$  [36]. For nickel complexes, a blue shift of the Soret band was observed, indicating that no structural distortions (characterized by redshifts). This observation is consistent with that due to the covalent radius of Ni (116 pm) that allows coordination without structural changes (“hole” in the center of ring 200 pm) [37]. Therefore, the observed shift can be attributed to its delocalized  $\pi$  electron density decreasing metalloporphyrins, increasing energy for the transition resulting in a blue shift of the Soret bands [38]. Furthermore, for complexes of Zn, a displacement of the Soret band towards red indicated structural deformation. The ionic radius of Zn (120 pm) may generate these distortions characterized by these shifts. The optimized structures [35] of the metal complexes are shown in Fig. S2 (supplementary material).

### Fluorescence quantum yield

The wide variety of applications that have received the porphyrin derivatives is based on an ability of the complexes to generate reactive oxygen species (ROS). A photosensitizer in its excited state can interact with triplet oxygen in the ground state to generate singlet oxygen [39]. This active molecule is responsible for many of the photoinduced oxidative processes in the different applications of porphyrins. Another important process that must be evaluated in as regards to the energy transfer from the photoexcited sensitizer is fluorescence emission. Information about the efficiency of fluorescence emission as a route deactivation is utilized when porphyrin compounds are used as tumor or cellular marker [40]. Therefore, measuring the quantum yields was performed to evaluate the potential use of these new porphyrin derivatives as photosensitizers.

The values of fluorescence quantum yields ( $\Phi_F$ ) of the synthesized compounds (1–8) were measured in water at a known

concentration and are summarized in Table 2. The fluorescence quantum yields were calculated using TPPS<sub>4</sub> as reference 0.12 [41].

The data of Table 2 clearly shows that include bulky groups reduces fluorescence quantum yield of the anionic compounds 1 ( $\Phi_F = 0.12$ ) and 4 ( $\Phi_F = 0.07$ ). Furthermore, it can be seen that the cationic charge in 6 ( $\Phi_F = 0.02$ ) provides an unfavorable effect on the fluorescence quantum yields. These results could be attributed to the observed structural distortions and promotion of intersystem crossing over the internal crossing [42]. Regarding the decrease for metal complexes, it has been reported [43] that metal coordination in porphyrins strongly affects the fluorescence. The heavy metals may increase the radiationless decay rate for the

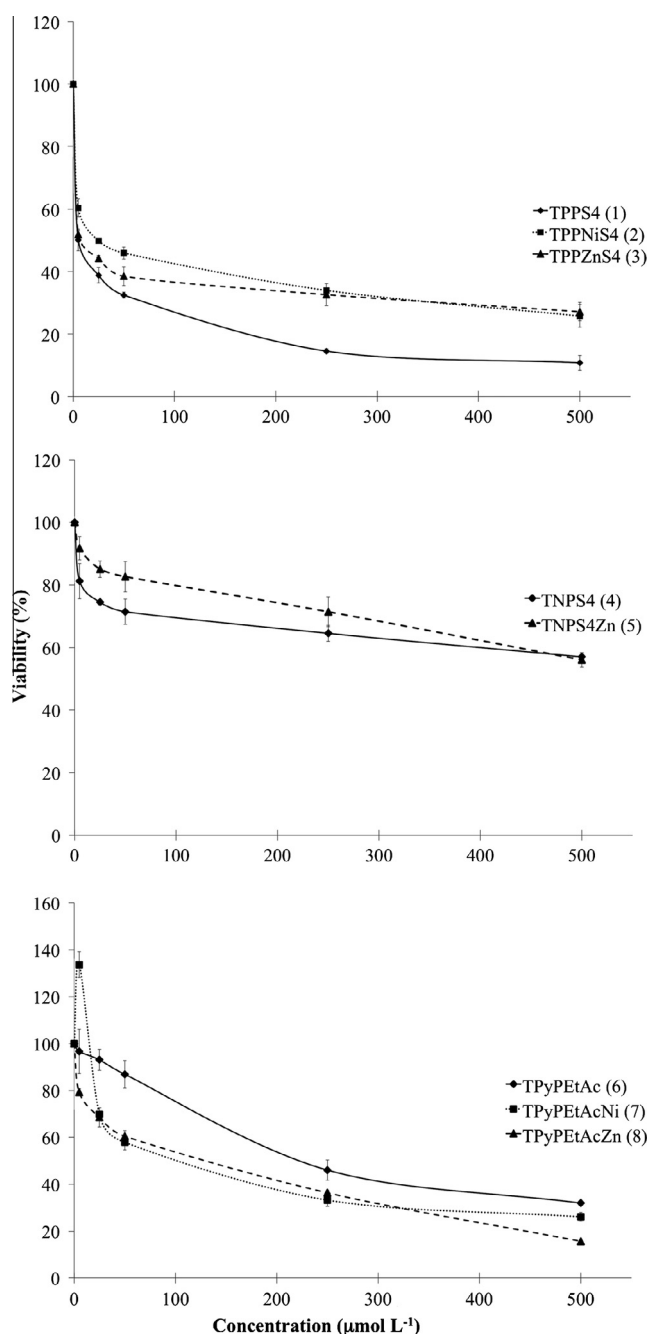


Fig. 5. Cell viability assay based on quantify ATP after irradiation (30 min) of *E. coli* cultures at different concentration of complexes 1–8. All values are mean of three independent assays. The error bars represent the standard deviation.

intersystem crossing to the excited triplet state, resulting in a decrease in the fluorescence quantum yield.

#### Singlet oxygen generation

Singlet oxygen ( $^1O_2$ ) is one of the reactive oxygen species generated photochemically of great interest. To evaluate the photosensitizing efficacy of the porphyrins synthesized, the singlet oxygen quantum yields ( $\Phi_A$ ) were measured. Rose Bengal ( $\Phi_A = 0.79$  in water) was used as the standard for determination of  $\Phi_A$  (Table 3). Photogeneration of singlet oxygen of 1–8 porphyrins ( $4 \times 10^{-5}$  mol  $l^{-1}$ ) was studied and quantified indirectly using histidine as  $^1O_2$  trapping to an irradiation time of 30 min (Fig. 3).

Quantification of singlet oxygen generated by the complexes (1–8) was used calibration curves through the method previously reported [22]. The results obtained for quantification and quantum yields are shown in Table 3.

Results of Table 3, the complexes with higher quantum yields of singlet oxygen formation (Type II photosensitizer) are 1, 2 and 6, with the TPPNiS<sub>4</sub> (2) porphyrin with near unit efficiency. Demonstrating that there is no linear relationship between the peripheral charges and efficiency in producing of singlet oxygen.

The generation of singlet oxygen involves the transfer of energy from the excited triplet state of the sensitizer to oxygen surrounding. In addition, the quantum yield of singlet oxygen is directly associated with a high lifetime of the triplet state as well as a low efficiency in the other deactivation mechanisms. In this regard, the metal coordination effect has been reported decreases the mean lifetime of the excited states increasing efficiency of other deactivation mechanisms [44]. This effect is clear for porphyrins 4, 5, 7 and 8 where the fluorescence and singlet oxygen quantum yields are low (Tables 2 and 3). Moreover, for complexes 1, 2 and 6 shows a high  $\Phi_A$  and a low  $\Phi_F$ , indicating that there is an increase in the efficiency of intersystem crossing [42].

#### Chemiluminescence assay

Efficiency in the photoinactivation of microorganisms mediated by photosensitizers, is directly related to producing ROS. In this sense, besides produce singlet oxygen determine efficiency to generate free radicals is necessary.

Quantifying the generated hydrogen peroxide after 15 min irradiation of the compounds 1–8 with NADH concentrations  $1.0 \times 10^{-4}$  mol  $l^{-1}$  of each complex were used. The determination was performed using chemiluminescence produced by the reaction

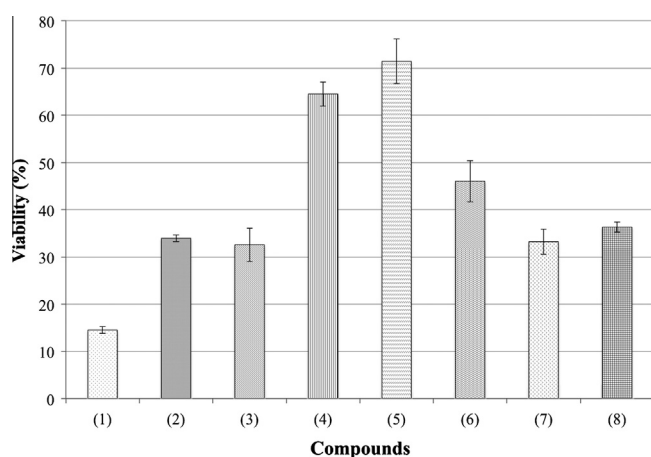


Fig. 6. Cell viability assay based on quantify ATP after irradiation (30 min) of *E. coli* cultures at  $250 \mu\text{mol } l^{-1}$  of complexes 1–8. All values are mean of three independent assays. The error bars represent the standard deviation.

of hydrogen peroxide with luminol. Photogeneration of  $H_2O_2$  as a function of light intensity (R.L.U: Relative Light Units) is shown in Fig. 4. Quantifying the  $H_2O_2$  (mol) produced by each complex is shown in Table 4. No production of free radicals was observed without irradiation (dark control).

Fig. 5 clearly shows that porphyrins with greater efficiency to produce free radicals are 3, 8 and 4. It can be inferred then that complexes 8 and 4 have as the only way of deactivation of triplet state production of radicals free (Type I photosensitizer), due to its low production of  $^1O_2$  and fluorescence. Efficiency in producing free radicals is associated with great mean lifetimes of the triplet state characteristic of photosensitizers with diamagnetic metals like Zn [45].

#### Photoinduced antibacterial activity on E. Coli

Fig. 5 shows a comparison of the photoinduced antibacterial action when compounds 1–8, at different concentrations, were irradiated during 30 min in the presence of *E. coli*. It is clearly seen that all compounds show activity dose-dependent photoinduced of the photosensitizer. It noted that the results obtained without radiation did not show significant changes in cell viability.

In Fig. 5, a low level of complex 7 ( $5 \mu\text{mol } l^{-1}$ ) is observed causes a bacterial growth, which can be associated with the Ni presence. Recently has been studied the influence of different metals such as Cu, Ni and Ag on the growth of microorganisms as trying to find new antibacterial alloys [46]. In this regard, it has been shown that low concentrations of Ni increase the growth rate of the bacterium *E. coli*, whereas at high concentrations, the effect is opposite [47]. Considering the effect of Ni on the metabolism of *E. coli*, and in the photoinactivation experiments the bacteria are under conditions of minimal maintenance, it can be inferred that low concentrations of Ni can be used to increase your metabolic activity. This effect is counteracted by the increased concentration obtaining the toxic effect of Ni.

In order to investigate the effect of peripheral charge, in each of complexes (1–8) comparing the results of viability with a concentration of  $250 \mu\text{mol } l^{-1}$  was performed. Results of these studies are shown in Fig. 6.

In Fig. 6, complexes with higher antibacterial activity (lower viability) are 1–3 consistent with high efficiency to produce ROS both Type I and Type II. In this respect, the complexes 1 and 2 show a high  $\Phi_A$  (Table 3) and a moderate production of free radicals (Table 4). Meanwhile, the complex 3 presents a high efficiency in producing free radicals and moderate  $\Phi_A$  (Tables 4 and 3 respectively). Furthermore, Figs. S1 and S2 show that the complexes 1–3 no significant structural deformations, thus reducing steric effects to interact with the microorganism, facilitating an efficient attack of the ROS produced [48]. In this way, we can infer that the complex 7 despite their low yields of ROS, due to its planarity explain its moderate antimicrobial activity. In this way, we can infer that the complex 7 despite their low yields of ROS due to its planarity, explain its moderate antimicrobial activity, while 8 overcomes its deformation with high production of free radicals (Table 4). Finally, the low cellular activity of complexes 4–6 is associated both with the low efficiency of ROS and its great structural deformity.

The results obtained in this work show a direct relationship between structure of porphyrins and antimicrobial activity. For a greater understanding of this relationship, would be necessary to conduct new studies focused on cellular mechanisms associated to this activity.

#### Conclusions

In conclusion, this work provides information on photodynamic activity of water-soluble porphyrins 1–8 with different charges on the periphery of the tetrapyrrole macrocycle and metal

coordination. Photochemical characterization showed that the mechanisms that the molecule deactivates excited state is influenced both by the presence of metals as well as by the structure of porphyrins. In this regard, the metal coordination decreases fluorescence quantum yields while the charges showed no clear trend. Determination of ROS showed that complex with Type II photosensitizing characteristics were **1**, **2** and **6** while the Type I was **3**, **8** and **4**. In this way, it was observed that coordination with diamagnetic metals favors the formation of free radicals, while complex without metals tend to produce singlet oxygen. The photoinduced antibacterial activity was closely related to the efficiency of formation of ROS and low molecular deformation. Complexes **1–3** showed the highest antibacterial activity. In this way, this work demonstrated that the design of efficient photosensitizers, an analysis must be made as to produce ROS as well as the molecular interaction of the drug with the target.

### Appendix A. Supplementary data

Supplementary data associated with this article can be found, in the online version, at <http://dx.doi.org/10.1016/j.saa.2014.07.053>.

### References

- [1] N. Shishkova, O. Kuznetsova, T. Berezov, *Cancer Biol. Med.* 9 (2012) 9–17.
- [2] J. Gray, G.M. Fullarton, *Photodiag. Photodyn. Ther.* 10 (2013) 561–565.
- [3] X. Ragas, M. Agut, S. Nonell, *Free Radic. Biol. Med.* 49 (2010) 770–776.
- [4] F. Vatansever, W.C. de Melo, P. Avci, D. Vecchio, M. Sadasivam, A. Gupta, R. Chandran, M. Karimi, N.A. Parizotto, R. Yin, G.P. Tegos, M.R. Hamblin, *FEMS Microbiol. Rev.* 37 (2013) 955–989.
- [5] T. Maisch, C. Bosl, R. Szeimies, N. Lehn, C. Abels, *Antimicrob. Agents Chemother.* 49 (2005) 1542–1552.
- [6] S.G. Bown, *Philos. Trans. Ser. A, Math. Phys. Eng. Sci.* 371 (2013) 20120371.
- [7] I. MacDonald, T. Dougherty, *J. Porphyrins Phthalocyanines* 5 (2001) 105–129.
- [8] E.M.P. Silva, C.I.V. Ramos, P.M.R. Pereira, F. Giuntini, M.A.F. Faustino, J.P.C. Tomé, A.C. Tomé, A.M.S. Silva, M.G. Santana-Marques, M.G.P.M.S. Neves, J.A.S. Cavaleiro, *J. Porphyrins Phthalocyanines* 16 (2012) 101–113.
- [9] O. Coppellotti, C. Fabris, M. Soncin, M. Magaraggia, M. Camerin, G. Jori, L. Guidolin, *Curr. Med. Chem.* 19 (2012) 808–819.
- [10] K. Komagoe, H. Kato, T. Inoue, T. Katsu, *Photochem. Photobiol. Sci.* 10 (2011) 1181–1188.
- [11] M.R. Hamblin, S.K. Sharma, G.B. Kharkwal, Chapter 4. Innovative design of antimicrobial photosensitizers, in: M.R. Hamblin, G. Jori (Eds.), *Photodynamic Inactivation of Microbial Pathogens: Medical and Environmental Applications*, 2011, pp. 69–82.
- [12] A. Almeida, A. Cunha, M.A.F. Faustino, A.C. Tomé, M.G.P.M.S. Neves, Chapter 5. Porphyrins as antimicrobial photosensitizing agents, in: M.R. Hamblin, G. Jori (Eds.), *Photodynamic Inactivation of Microbial Pathogens*, 2011, pp. 83–160.
- [13] D. Lazzeri, M. Rovera, L. Pascua, E.N. Durantin, *Photochem. Photobiol.* 80 (2004) 286–293.
- [14] S. Banfi, E. Caruso, L. Buccafurni, V. Battini, S. Zazzaron, P. Barbieri, V. Orlandi, *J. Photochem. Photobiology B85* (2006) 28–38.
- [15] A. Adler, F. Longo, J. Finarelli, J. Goldmacher, J. Assour, L. Korsakoff, *J. Org. Chem.* 32 (1967). 476–476.
- [16] R.G. George, M. Padmanabhan, *Polyhedron* 24 (2005) 679–684.
- [17] M. Berezin, N. Berezina, A. Semeikin, A. V'Yugin, *Russ. J. Gen. Chem.* 77 (2007) 1955–1958.
- [18] T. Srivastava, M. Tsutsui, *J. Org. Chem.* 38 (1973). 2103–2103.
- [19] O. Herrmann, S.H. Mehdi, A. Corsini, *Can. J. Chem.* 56 (1978) 1084–1087.
- [20] J.G. Calvert, J.N. Pitts, *Photochemistry*, Wiley, New York, 1966.
- [21] M. Durmus, T. Nyokong, *Spectrochim. Acta Part A Mol. Biomol. Spectrosc.* 69 (2008) 1170–1177.
- [22] T. Zoltan, F. Vargas, C. Izzo, *Anal. Chem. Insights* 2007 (2007) 1–8.
- [23] W. Lovell, D. Sanders, *Toxicol. In Vitro* 4 (1990) 318–320.
- [24] W.R. Haag, J. Hoigne, E. Gassman, A.M. Braun, *Chemosphere* 13 (1984) 631–640.
- [25] J. Allen, C. Gossett, S. Allen, *J. Photochem. Photobiology B32* (1996) 33–37.
- [26] J.J.M. Lamberts, D.R. Schumacher, D.C. Neckers, *J. Am. Chem. Soc.* 106 (1984) 5879–5883.
- [27] A. Ogunsipe, J. Chen, T. Nyokong, *New J. Chem.* 28 (2004) 822–827.
- [28] H. Lundqvist, C. Dahlgren, *Free Radical Biol. Med.* 20 (1996) 785–792.
- [29] F. Vargas, C. Rivas, N. Contreras, A. Silva, L. Ojeda, M. Velásquez, G. Fraile, *Pharmazie* 58 (2003) 818–823.
- [30] Y. Gülüzar, A. Demiryürek, S.-E. İnci, K. İlker, *Br. J. Pharmacol.* 124 (1998) 905–910.
- [31] A. American Type Culture Collection, Product Description: *Escherichia coli* ATCC® 8739™, 2007. <<http://www.atcc.org/ATCCAdvancedCatalogSearch/ProductDetails/tabid/452/Default.aspx?ATCCNum=8739&Template=bacteria>>.
- [32] S. Zakavi, R. Omidyan, L. Ebrahimi, F. Heidarzadi, *Inorg. Chem. Commun.* 14 (2011) 1827–1832.
- [33] J.A. Shelnett, X.-Z. Song, J.-G. Ma, S.-L. Jia, W. Jentzena, C.J. Medforth, *Chem. Soc. Rev.* 27 (1998) 31–41.
- [34] P. Bhyrappa, M. Sankar, B. Varghese, P. Bhavana, *J. Chem. Sci. (Bangalore, India)* 118 (2006) 393–397.
- [35] M.D. Hanwell, D.E. Curtis, D.C. Lonie, T. Vandermeersch, E. Zurek, G.R. Hutchison, *J. Cheminf.* 4 (2012) 17.
- [36] K.M. Smith, J.E. Falk, *Porphyrins and metalloporphyrins*, New ed. based on the original volume by J.E. Falk; edited by Kevin M. Smith ed., Elsevier Scientific Pub. Co., Netherlands, 1975.
- [37] J.E. Huheey, *Inorganic Chemistry: Principles of Structure and Reactivity*, third Ed., Harper & Row Publishers, New York, 1983.
- [38] W. Zheng, N. Shan, L. Yu, X. Wang, *Dyes Pigm.* 77 (2008) 153–157.
- [39] P. Agostinis, K. Berg, K.A. Cengel, T.H. Foster, A.W. Girotti, S.O. Gollnick, S.M. Hahn, M.R. Hamblin, A. Juzeniene, D. Kessel, M. Korbelik, J. Moan, P. Mroz, D. Nowis, J. Piette, B.C. Wilson, J. Golab, *CA Cancer J. Clin.* 61 (2011) 250–281.
- [40] A.E. O'Connor, M.M. Mc Gee, Y. Likar, V. Ponomarev, J.J. Callanan, F. O'Shea D, A.T. Byrne, W.M. Gallagher, *Int. J. Cancer* 130 (2012) 705–715.
- [41] K. Kalyanasundaram, M. Neumannspallart, *J. Phys. Chem.* 86 (1982) 5163–5169.
- [42] Z. Valicsek, O. Horváth, K. Patonay, *J. Photochem. Photobiology A226* (2011) 23–35.
- [43] T. Wijesekera, D. Dolphin, Some preparations and properties of porphyrins, in: D. Kessel (Ed.), *Methods in Porphyrin Photosensitization*, Springer, US, 1985, pp. 229–266.
- [44] T. Maisch, J. Baier, B. Franz, M. Maier, M. Landthaler, R. Szeimies, W. Baumler, *Proc. Nat. Acad. Sci. USA* 104 (2007) 7223–7228.
- [45] W. Sharman, C. Allen, J. van Lier, S. Lester Packer, Helmut, *Methods Enzymol.* 319 (2000) 376–400.
- [46] S. Wilks, H. Michels, C. Keevil, *Int. J. Food Microbiol.* 105 (2005) 445–454.
- [47] C. Long-Fei Wu, *Environ. Health Perspect.* 102 (1994) 297–300.
- [48] A.N. Vzorov, D.W. Dixon, J.S. Trommel, L.G. Marzilli, R.W. Compans, *Antimicrob. Agents Chemother.* 46 (2002) 3917–3925.